






Transits of Inclined Exomoons—Hide and Seek and an Application to Kepler-1625

David V. Martin¹ , Daniel C. Fabrycky , and Benjamin T. Montet² 

Department of Astronomy and Astrophysics, University of Chicago, 5640 South Ellis Avenue, Chicago, IL 60637, USA; davidmartin@uchicago.edu

Received 2018 December 22; revised 2019 February 26; accepted 2019 February 27; published 2019 April 19

Abstract

A Neptune-sized exomoon candidate was recently announced by Teachey & Kipping, orbiting a 287 day gas giant in the Kepler-1625 system. However, the system is poorly characterized and needs more observations to be confirmed, with the next potential transit in 2019 May. In this Letter, we aid observational follow up by analyzing the transit signature of exomoons. We derive a simple analytic equation for the transit probability and use it to demonstrate how exomoons may frequently avoid transit if their orbit is larger than the stellar radius and sufficiently misaligned. The nominal orbit for the moon in Kepler-1625 has both of these characteristics, and we calculate that it may only transit $\approx 40\%$ of the time. This means that ≈ 6 non-transits would be required to rule out the moon's existence at 95% confidence. When an exomoon's impact parameter is displaced off the star, the planet's impact parameter is displaced the other way, so larger planet transit durations are typically positively correlated with missed exomoon transits. On the other hand, strong correlations do not exist between missed exomoon transits and transit timing variations of the planet. We also show that nodal precession does not change an exomoon's transit probability and that it can break a prograde-retrograde degeneracy.

Key words: eclipses – methods: analytical – Moon – planets and satellites: detection – planets and satellites: dynamical evolution and stability – planets and satellites: general

1. Introduction

In the solar system our understanding of the planets is enriched by our understanding of their moons. The Moon is thought to influence Earth's habitability (Laskar et al. 1993). The Galilean moons help constrain the early evolution of Jupiter (Heller et al. 2015; Ronnet et al. 2018). The equatorial alignment of Uranus's moons helps us understand the origin of the planet's tilt (Kegerreis et al. 2018). As a community we would benefit immensely from conducting similar science for moons of extrasolar planets (exomoons).

Detecting analogs of the solar system moons is challenging due to their small size. Photometry is thought to be the most promising technique (Kipping et al. 2009), either through observing individual moon transits (Sartoretti & Schneider 1999), multiple averaged moon transits (Simon et al. 2012; Heller 2014; Teachey et al. 2017), or inferring the moon's existence based on the planet's transit timing variations (TTVs) and transit duration variations (TDVs; Sartoretti & Schneider 1999; Kipping 2009a, 2009b, 2011; Heller et al. 2016). Other techniques with potential include gravitational microlensing (Bennett et al. 2014; Hwang et al. 2018) and observations of self-luminous giant exoplanets to detect a variation in polarization (Sengupta & Marley 2016) or in radial velocity (Vanderburg et al. 2018).

The most plausible exomoon to date is in the Kepler-1625 system. The planet (Kepler-1625b) itself is unremarkable: a gas giant on a 287 day orbit. The surprise, however, is the size of the moon (Kepler-1625b-i), as it is potentially similar in mass and radius to Neptune. Such a large moon is without precedent in our solar system, but one must remember that so were the first exoplanet discoveries.

The moon was originally suspected based on three planet transits within the original *Kepler* mission (Teachey et al. 2017;

Heller 2018). Asymmetries in the transit profile teased the presence of a moon, but neither TTVs nor TDVs were detected to confirm it. The moon's existence became more likely after a fourth planetary transit was captured by the *Hubble Space Telescope* (*HST*; Teachey & Kipping 2018). The planet transit was 70 minutes early, although no TDV was detected. Furthermore, there is a shallow dip in the light curve after the egress of the planet transit: a potential moon transit. Table 1 contains basic system parameters used in our Letter, but we refer the reader to Teachey & Kipping (2018) for significantly more detail.

In this Letter we are agnostic about the reality of this particular exomoon. Both Teachey & Kipping (2018) and subsequent analysis by Heller et al. (2019) encourage new observations in order to consider the moon confirmed. In this Letter we aid such future observations by analyzing the detectability of exomoons, both in general and for Kepler-1625b-i specifically. We quantify previous intuition that some moons are not guaranteed to transit every time their host planet does (Sartoretti & Schneider 1999; Martin 2017). Missed transits typically occur when the moon's orbit is both wider than the stellar diameter and significantly misaligned to the planet's orbital plane. The best-fitting, albeit loosely constrained orbit for Kepler-1625b-i has both of these characteristics. Furthermore, within our own solar system we know of Triton, which is on a highly misaligned, in fact retrograde, orbit (Figure 1).

In this Letter we derive an analytic transit probability for exomoons of transiting planets (Section 2), which accounts for both misalignment and a dynamically varying exomoon orbit. We then test the correlation between the presence/absence of moon transits and the TTV and TDV signature of the planet (Section 3). We apply our work to both exomoons in general and the Kepler-1625 system specifically (Section 4). The Letter ends with a brief discussion (Section 5).

¹ Fellow of the Swiss National Science Foundation.

² NASA Sagan Fellow.

Table 1
Parameters of the Kepler-1625 Exomoon Candidate System

Param.	Unit	Value	1 σ Min	1 σ Max	Note
Host Star					
m_*	(M_\odot)	1.04	0.98	1.12	
R_*	(R_\odot)	1.73	1.51	1.97	
Planet					
m_P	(M_{Jup})	6.85	1.2	12.5	(a)
R_P	(R_{Jup})	1.04	0.90	1.18	
T_P	(days)	287.37278	287.37213	287.37353	
a_P	(au)	0.87	0.85	0.89	(b)
b_P		0.104	0.038	0.188	
I_P	(deg)	89.94	89.88	89.98	(c)
Ω_P	(deg)	0	0	0	(c)
Moon					
m_M	(M_\oplus)	36.2	4.4	68	(a)
R_M	(R_\oplus)	4.90	4.18	5.69	
T_M	(days)	22	13	39	
a_M	(au)	0.022	0.017	0.030	(d)
I_M	(deg)	42	24	57	(e)
Ω_M	(deg)	0	-83	142	(e)
Relative Orbit					
$ 90 - I_M $	(deg)	48	33	66	(f)

Note. Parameter key: m : mass, R : radius, T : period, a : semimajor axis, b : impact parameter, I : inclination, Ω : longitude of the ascending node. (a) No nominal value is given for the planet or moon mass, only upper and lower bounds, so the value that we provide here is simply an average. (b) Teachey & Kipping (2018) gave $a_P = 0.98^{+0.14}_{-0.13}$ au, but this is inconsistent with their values for $T_P = 287$ days and $M_* = 0.98^{+0.08}_{-0.06} M_\odot$ so we recalculate a_P and our value matches Heller (2018). (c) I_P is not given by Teachey & Kipping (2018); calculated from our value of a_P and the given values of b_P . $\Omega_P = 0^\circ$ arbitrarily because transits are not sensitive to both Ω_P and Ω_M individually, only $\Delta\Omega$. (d) Not given by Teachey & Kipping (2018); calculated from their values of $a_M/R_P = 45^{+10}_{-5}$. (e) We take I_M and Ω_M to be calculated with respect to the observer, although we note that Ω_M is essentially unconstrained by the data, with a 225° 1σ confidence interval. The inclination value is also modulo 90° , i.e., a degeneracy exists. (f) Equivalent to ΔI from Equation (2) with $\Omega_M = 0^\circ$ and $I_P = 90^\circ$. We use this as the moon’s mutual inclination because Teachey & Kipping (2018) did not give a value and Ω_M is so poorly constrained.

2. Exomoon Transit Probability

2.1. Transit Geometry

The transit geometry is shown in Figure 2. The observer looks from the positive z -axis at the (x, y) sky plane centered on the star. The planet orbit is modeled by a straight line from left to right (positive x direction), vertically offset by the impact parameter $b_P = a_P \cos I_P / R_*$. This assumes $a_P \gg R_*$ and $m_P \gg m_M$,⁴ and throughout this Letter we also assume circular orbits, i.e., $e_P = e_M = 0$. The planet’s orbit would be rotated clockwise by Ω_P , but we arbitrarily set $\Omega_P = 0$ as the transit geometry are only sensitive to $\Delta\Omega = \Omega_M - \Omega_P$.

The position of the moon at the time of the planet’s transit midpoint across the star is fundamental to the transit

phenomenon. Neglecting eccentricity, its projected orbit is an ellipse with major axis a_M and a minor axis $a_M |\cos I_M|$, rotated counter-clockwise by Ω_M and offset vertically by $b_P R_*$:

$$\begin{aligned} & \begin{bmatrix} x_M(f_M) \\ y_M(f_M) \end{bmatrix} \\ &= \begin{bmatrix} a_M(\cos \Omega_M \cos f_M - \cos I_M \sin \Omega_M \sin f_M) \\ a_M(\sin \Omega_M \cos f_M + \cos I_M \cos \Omega_M \sin f_M) + b_P R_* \end{bmatrix}, \end{aligned} \quad (1)$$

where f_M is the true anomaly of the moon. It is important to remember that f_M is the orbital phase of the moon defined within its orbital plane, *not* with respect to our (x, y) coordinate system. In Figure 2 the moon is misaligned and prograde with the planet’s orbit and projects a counter-clockwise motion. In Figure 6 we however note that a degeneracy exists between prograde and retrograde moons (see Section 5.1). The mutual inclination between the moon and the planet’s orbit (not equator) is

$$\cos \Delta I = \cos \Delta\Omega \sin I_M \sin I_P + \cos I_M \cos I_P. \quad (2)$$

The moon will transit the star on a given planet transit when $|y_M(f_M)| < R_*$. To make this criterion easier to solve, we consolidate the expression in Equation (1) for y_M from two trigonometric functions of f_M to one:

$$\begin{aligned} y_M(f_M) &= a_M \sqrt{\sin^2 \Omega_M + \cos^2 I_M \cos^2 \Omega_M} \\ &\quad \times \cos \left(f_M - \arctan \left[\frac{\cos I_M}{\tan \Omega_M} \right] \right) + b_P R_* \\ &\approx a_M |\sin \Delta I| \cos \left(f_M - \arctan \left[\frac{\cos I_M}{\tan \Omega_M} \right] \right) + b_P R_*, \end{aligned} \quad (3)$$

We note that while the second line of Equation (3) contains b_P , hence implying that I_P is not exactly 90° , the approximation $\sqrt{\sin^2 \Omega_M + \cos^2 I_M \cos^2 \Omega_M} \approx |\sin \Delta I|$ is derived from Equation (2) using $I_P = 90^\circ$. However, the end result is a negligible difference between the two lines in Equation (3).

The exomoon transit probability is calculated as the fraction of angles f_M that correspond to $|y_M| < R_*$. The phase shift of $\arctan[\cos I_M / \tan \Omega_M]$ in Equation (3) does not affect this fraction, and hence we simplify Equation (3) by defining $f'_M = f_M - \arctan[\cos I_M / \tan \Omega_M]$. The function $y_M(f'_M)$ is symmetric over $f'_M = 180^\circ$. Between 0 and 180° we define the range of transits to be $[A, B]$, where

$$A = \begin{cases} 0 & \text{if } b_P R_* + a_M |\sin \Delta I| < R_* \\ \arccos \left[\frac{R_* (1 - b_P)}{a_M \sin \Delta I} \right] & \text{if } b_P R_* + a_M |\sin \Delta I| > R_* \text{ (can miss above star),} \end{cases} \quad (4)$$

and

$$B = \begin{cases} 180^\circ & \text{if } b_P R_* - a_M |\sin \Delta I| > -R_* \\ \arccos \left[\frac{-R_* (1 + b_P)}{a_M \sin \Delta I} \right] & \text{if } b_P R_* - a_M |\sin \Delta I| < -R_* \text{ (can miss below star).} \end{cases} \quad (5)$$

If f'_M (and hence y_M) is static during the planet’s transit then the exomoon transit probability is simply the ratio $p_M = (B - A) / 180^\circ$. However, this static assumption is only applicable when $T_M \gg \tau_P$, where τ_P is the planet’s transit

³ Very tight-orbiting planets are thought unlikely to host moons anyway (Namouni 2010).

⁴ Care must be taken when generalizing our work to “binary planets” (Lewis et al. 2015), although our work is likely applicable to “moon-moons” (Forgan 2018), “moon-moon-moons,” or indeed moon”.

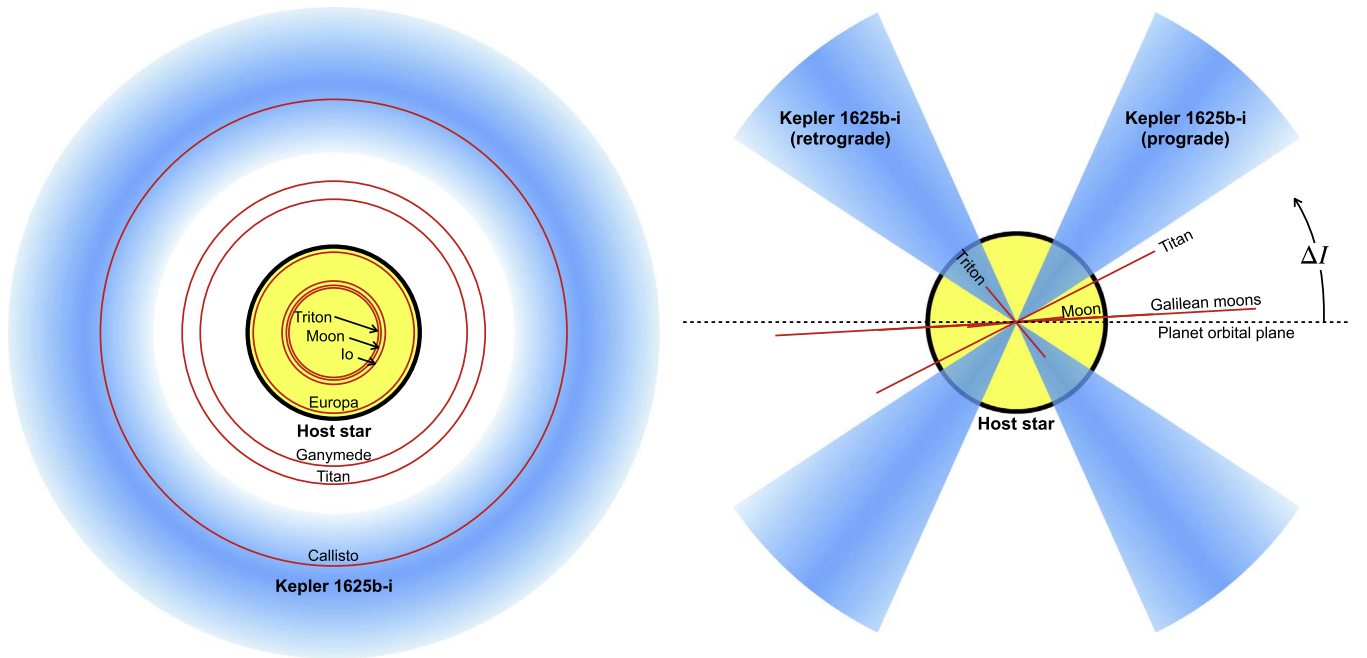


Figure 1. Left: orbits of the seven most massive solar system moons (red) and the exomoon candidate Kepler-1625b-i (the shaded blue region denotes the 1σ a_M error bars) compared with the host star disk, ignoring eccentricity. Right: mutual inclination (ΔI) measured counter-clockwise from the planet orbital plane (black dashed horizontal line) to the moon orbital plane. The massive solar system moons are shown as individual red lines, although most closely overlap. For Kepler-1625 we estimate $\Delta I \approx 90^\circ - I_M$ from Equation (2) with $\Delta\Omega = 0$ and $I_P = 90^\circ$. For the error in ΔI we take the given 1σ errors for I_M . A blue shaded region shows the 1σ confidence interval and is mirrored for retrograde. Note that Titan is actually almost coplanar to its host Saturn’s equator, but the planet is tilted by $\Delta I = 27^\circ$ from its orbital plane.

duration:

$$\tau_P = \frac{T_P}{\pi} \arcsin \left(\frac{R_* \sqrt{1 - b_P^2}}{a_P} \right), \quad (6)$$

To approximately account for shorter-period moons we add to p_M the fraction of the orbit covered during the planet’s transit: τ_P/T_M . With this, our derived exomoon transit probability is

$$p_M = \min \left[\frac{B - A}{180^\circ} + \frac{\tau_P}{T_M}, 1 \right]. \quad (7)$$

2.2. Orbital Dynamics

The orbit of an exomoon may be subject to various dynamical perturbations. When the moon and planet orbits are misaligned, one such effect is a nodal precession induced by the three-body interactions between the Sun, planet, and moon. From Mardling (2010) the rate of precession is

$$T_{\text{prec}} = \frac{4}{3} \frac{m_P + m_*}{m_*} \frac{T_P^2}{T_M} \frac{1}{\cos \Delta I}. \quad (8)$$

This effect may be quenched by a competing torque on the moon’s orbit induced by the equatorial bulge of the planet. Burns (1986) calculated a critical moon semimajor axis, for which the dynamics of interior orbits are dominated by the planet’s equatorial bulge:

$$a_{M,\text{crit}} = \left(\frac{2J_2 R_P^2 a_P^3 m_P}{m_*} \right)^{1/3}, \quad (9)$$

where J_2 is the first gravitational harmonic. See also Boué & Laskar (2006) and Tremaine et al. (2009) for more details. In this Letter we are predominantly interested in moons that are long-period and misaligned (such that moon transits are sometimes missed) and planets that are short-period (so planet

transits are more frequent). For such moons the dominant effect is a three-body nodal precession. The Earth’s moon exhibits three-body nodal precession with a period of 17.9 yr (according to Equation (8)). For Kepler-1625 $a_{M,\text{crit}} = 0.008$ au, which is almost three times less than the nominal value $a_M = 0.022$ au, and hence we also expect three-body nodal precession in this system, with a calculated period of 20.5 yr.

With respect to the orbital plane of the planet, which remains (essentially) fixed, nodal precession makes the moon orbit circulate at a constant rate given by Equation (8), while maintaining a constant mutual inclination ΔI . With respect to the observer, Martin (2017) showed that I_M librates over time t around the constant I_P according to

$$I_M(t) = \Delta I \cos \left[\frac{2\pi}{T_{\text{prec}}} (t - t_0) \right] + I_P, \quad (10)$$

where t_0 corresponds to $I_{M,0}$. With respect to the observer, $\Omega_M(t)$ also librates and can be calculated by combining Equations (2) and (10).

A complication to the nodal precession arises in highly misaligned orbits, such that $|90^\circ - \Delta I| \lesssim 50^\circ$. In such cases Kozai–Lidov cycles occur, which cause ΔI and e_M vary, even for initially circular orbits (Lidov 1961, 1962; Kozai 1962).

The expression for y_M in Equation (3) *does* depend on the time-dependent quantities I_M and Ω_M . However, these quantities only phase shift f_M and *do not* change the fractional range of f_M corresponding to transits, which is why they could be ignored when calculating the quantities A (Equation (4)) and B (Equation (5)). These quantities are functions of ΔI , but this is constant⁵ for

⁵ To be precise, ΔI is only constant under the secular regime, i.e., when calculations are made that average over the orbital periods. There do exist short-term variations on the timescales of T_M and T_P , but these are on order $\approx 2\%$ variations.

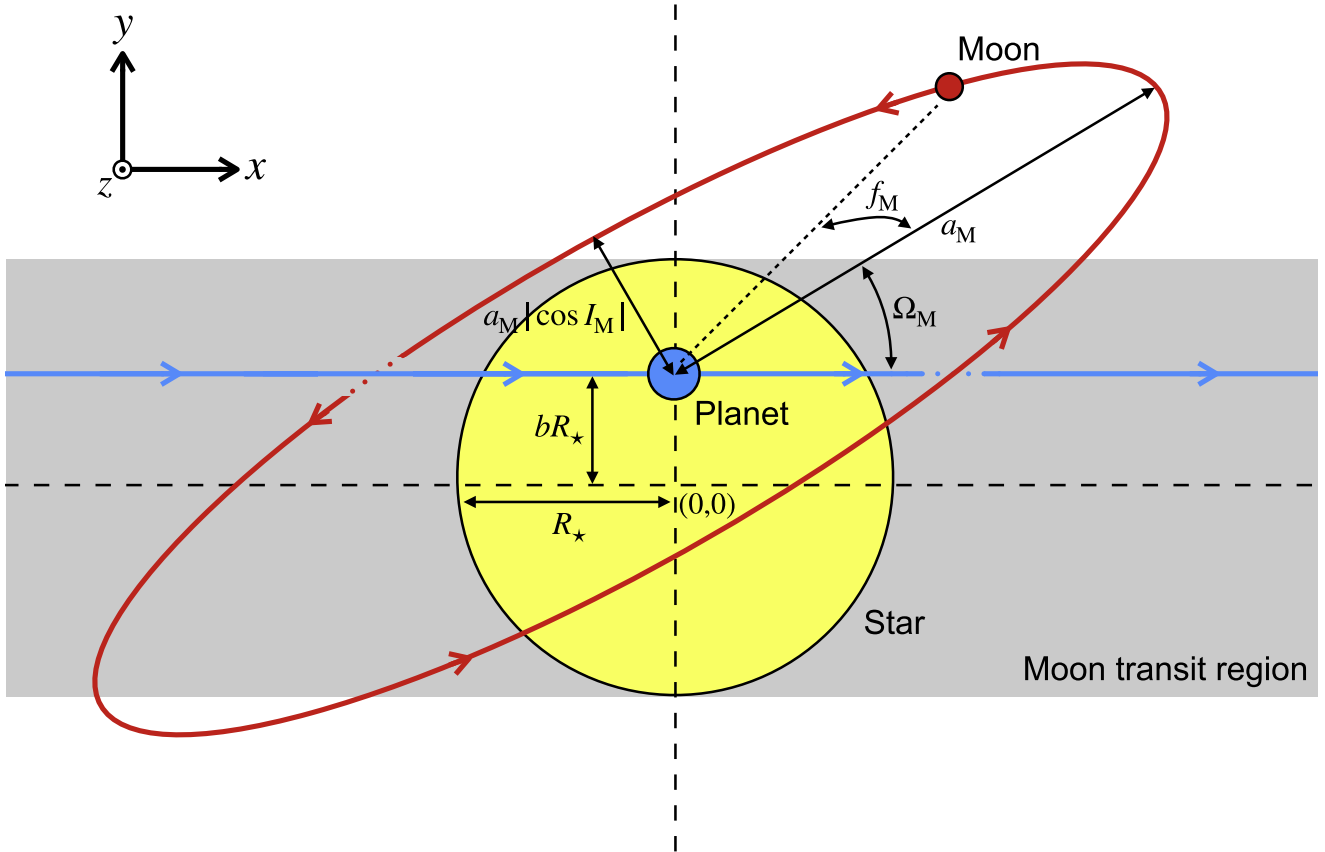


Figure 2. Observer’s view of a transiting exoplanet (blue), its host star (yellow), and exomoon (red). Moons within the gray region will transit the star. Dotted regions of the moon and planet orbits show where those orbits pass behind the projected orbit of the other body.

orbits that are circular and without Kozai–Lidov cycles. Overall, we demonstrate that in our simplified setup the exomoon transit probability p_M is constant during the moon’s precession period.

2.3. Accuracy of the Analytic Solution

We run n -body simulations for a suite of 1000 randomized transiting planet plus moon systems and calculate a numerical transit probability as the ratio of moon to planet transits. The masses are $m_* = 1M_\odot$, $m_P \in [0.1, 3]M_{\text{Jup}}$, $m_M \in [0.1, 17]M_\oplus$, using log-uniform distributions. The planet radii are calculated using the mass–radius relation of Bashi et al. (2017): $R/R_\oplus = (m/M_\oplus)^{0.55}$ for $m/M_\oplus < 124$ and $R/R_\oplus = (m/M_\oplus)^{0.01}$ for $m/M_\oplus \geq 124$. The orbital parameters for the planet are $T_P \in [200, 500]$ days, $e_P = 0$, $\Omega_P = 0$, $b_P \in [0, 0.9]$, and $f_P \in [0^\circ, 360^\circ]$. The orbital parameters for the moon are $T_M \in [1, 50]$ days, $e_M = 0$, $f_M \in [0^\circ, 360^\circ]$. The mutual inclination is drawn from $\Delta I \in [0^\circ, 40^\circ]$. We randomly choose the starting phase of the precession period by calculating I_M in Equation (10) with a uniformly random phase between $\in [0^\circ, 360^\circ]$ and I_P calculated from the randomly chosen b_P . We then calculate Ω_M from Equation (2).

Each simulation is run over a time span of $100 \times T_P$ using a fourth-order Runge–Kutta integrator with a fixed step size of 30 minutes, chosen to match *Kepler*’s long-cadence observations. Across all 1000 simulations, the median percentage error between the analytic and numerical transit probabilities is 1.2%. For 626 of the simulations the numerical transit probability is less than 1 (i.e., at least one missed moon

transit), and for these simulations the median error is 4.0%. Contributions to the error include perturbations to the moon’s orbit, mean motion resonances, other period-ratio effects that may alias the moon transit sequence, any simplifications in the derivation of Equation (7), and counting statistics of the numerically calculated transit probability.

3. Planet Transit Timing and Duration Variations

An isolated, unperturbed planet would transit the star with perfect periodicity, T_P . However, the presence of the moon can induce TTVs and TDVs on the planet. The main cause is a small “wobble” of the planet around the planet–moon barycenter, on top of the planet’s larger-scale orbit around the star–planet barycenter. This is a Keplerian effect (i.e., it occurs with static orbits). We briefly discuss the origin of the barycentric TTVs and TDVs in Section 3.1, and direct the reader to the seminal papers of Kipping (2009a, 2009b) for a much more thorough treatment, included detailed analytic equations. A secondary contribution to TTVs and TDVs is from non-Keplerian effects, i.e., perturbations to the orbital elements. We do not discuss these effects but they are naturally included in our n -body simulations. Finally, we do not discuss the TTVs and TDVs of the moon itself, but they are expected to significantly larger than those of the planet.

3.1. Origins of Barycentric TTVs and TDVs

A planet exhibits a TTV when slightly offset along the *horizontal axis* (i.e., parallel with its transit chord). This change

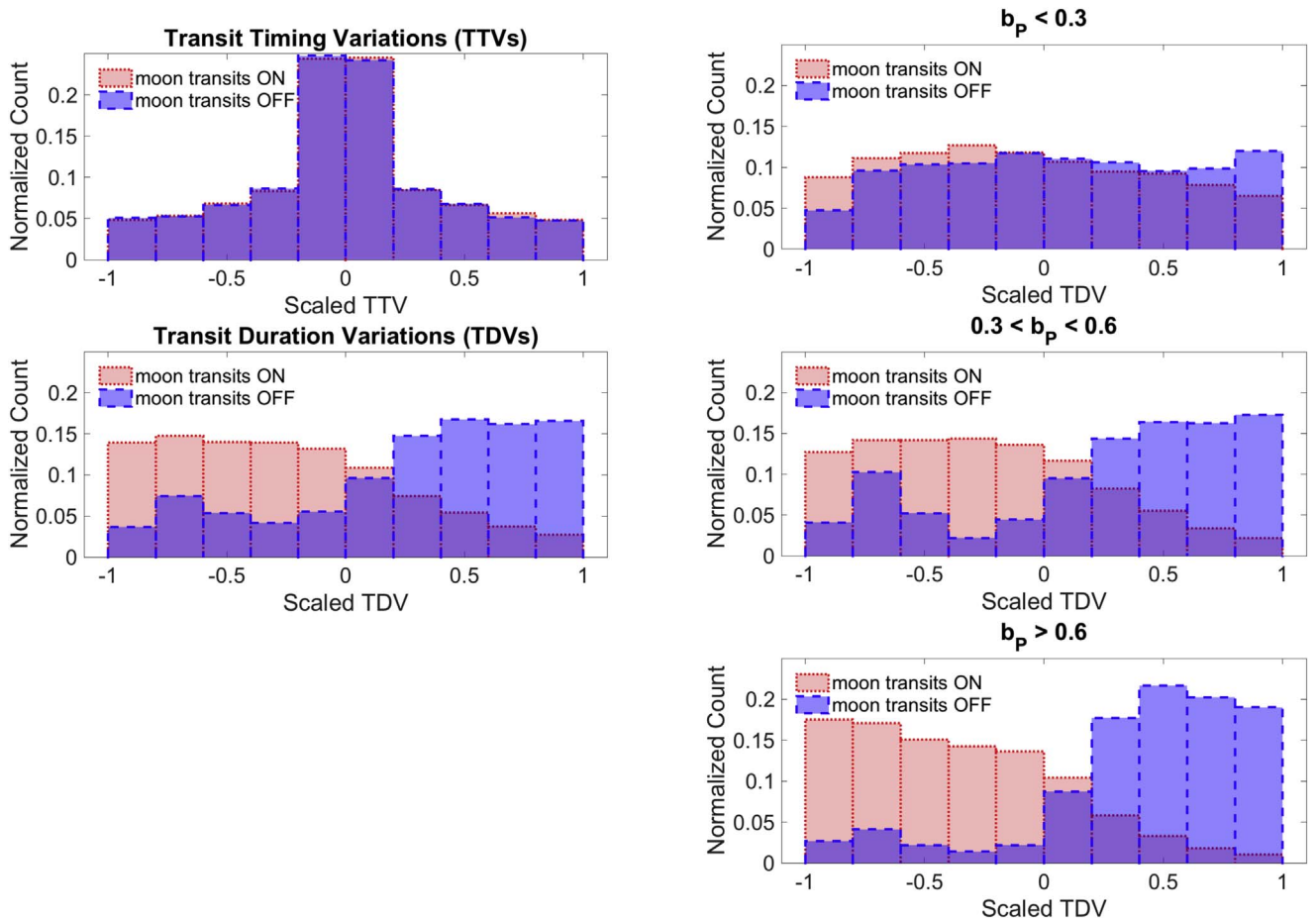


Figure 3. Left: normalized histograms of TTVs and TDVs, scaled by the maximum amplitude in each simulation and separated to when the moon does transit (moon transits ON, red) and does not transit (moon transits OFF, blue). The TTVs and TDVs are calculated in the n -body simulations presented in Section 2.3, only taking the 626/1000 simulations with at least one missed moon transit. Right: same TDV results but separated into small (top), moderate (middle), and high (bottom) planet impact parameters.

adds or subtracts to the time taken to reach the transit midpoint. A horizontal offset is induced by the planet’s wobble around the planet–moon barycenter. The TTV is calculated as the time taken for the planet to traverse this offset at its orbital velocity around the star of $v_{P,*} = 2\pi a_P/T_P$.

A planet exhibits a TDV for two different reasons. First, the planet’s motion around the planet–moon barycenter has a velocity $v_{P,M} = 2\pi a_M m_M / [(m_P + m_M) T_M]$. The *horizontal* component of this velocity may be additive or subtractive to $v_{P,*}$, and hence when the planet transits it may be moving a little faster or slower than average, causing the transit duration to vary. Kipping (2009b) called this the “V-TDV.”

The second cause of a TDV is a *vertical* offset of the planet’s position (i.e., perpendicular to its transit chord) due to the barycentric reflex motion induced by the moon. This changes b_P , hence changing τ_P by Equation (6). Kipping (2009b) called this the “TIP-TDV.”

3.2. Connecting TTVs and TDVs with Moon Transit Occurrence

We use the Section 2.3 n -body simulations to test the correlation between moon transits and planet TTVs and TDVs. We only take the 626/1000 simulations that have at least one missed moon transit. For each simulation we calculate numerically the TTVs and TDVs, which we scale by dividing

each value by the maximum absolute value for the simulation. We collate the scaled TTVs and TDVs for the simulations, separate them by moon transit occurrence, and show the results in a histogram in Figure 3 (left).

For TTVs there is typically no difference between when the moon does and does not transit. There are two main reasons for this. First, occurrence of a moon transit is a function of its vertical position (y_M), yet the TTV signal is a function of the moon’s horizontal position (x_M). Consider Figure 2. A positive x_M displaces the planet to the left and hence induces a positive TTV (late transit), and vice-versa. We see that positive x_M values correspond to both cases where the moon does and does not transit (only misses above the star). Negative x_M values largely correspond to the moon transiting, but there is also a small parameter space for missing transits, both above and below the star. In Figure 2, when averaged over all x_M there will be preference for missed transits to correspond to positive values of x_M , and hence positive TTVs. However, this trend will be weak except for small a_M/R_* , and in that case it would be rare for the moon to avoid transit anyway. The second consideration is that nodal precession of the moon rotates its orbit. After $0.5T_{\text{prec}}$ the moon orbit in Figure 2 will be mirrored horizontally, in which case missed moon transits will now typically correspond to negative values of x_M . Our n -body simulations cover multiple precession periods, and hence any

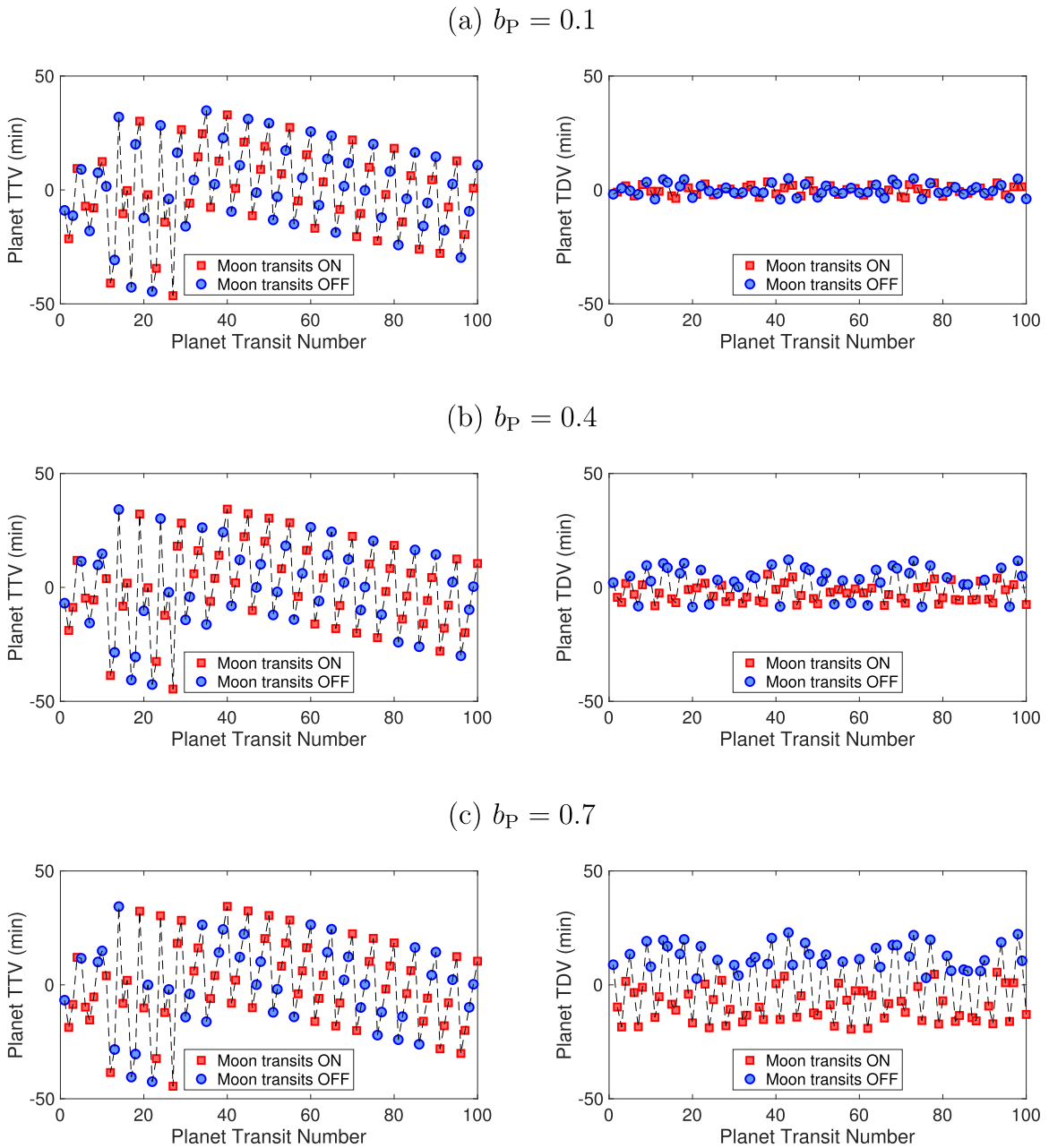


Figure 4. TTVs (left) and TDVs (right) for a $5M_{\oplus}$, $2R_{\oplus}$ moon with $T_M = 20$ days ($a_M = 3.05R_{\odot}$) around a $1M_{\text{Jup}}$, $1R_{\text{Jup}}$ planet with $T_P = 1$ yr orbit around a $1M_{\odot}$, $1R_{\odot}$ star, with misalignment of $\Delta I = 30^\circ$ and planet impact parameters 0.1 (a), 0.4 (b), and 0.7 (c). All simulations start with $\Omega_M = 0^\circ$, $f_P = 0^\circ$, and $f_M = 50^\circ$. Red indicates that moon transits occur, while blue indicates that they did not.

small short-term TTV-moon transit correlations are averaged out.

For TDVs the results contrastingly show a clear difference in the TDV distribution with and without moon transits. This matches Figure 2; the moon misses transit when in the uppermost and lowermost parts of its orbit, but the upper region is larger due to the asymmetric vertical offset. When the moon is in this upper region the planet is displaced slightly downward toward the stellar center, and hence takes longer to transit (a positive TDV). This does not change throughout the nodal precession period.

The TDV-transit correlation is only prominent when b_P is significantly non-zero. In Figure 3 (right) we split the simulations into $b_P \in [0, 0.3]$, $[0.3, 0.6]$, and $[0.6, 0.9]$. The

correlation between TDVs and moon transits disappears for small impact parameters. There are two reasons for this. First, for the same vertical offset induced by the moon the change in the path length across the star is less when the planet passes near the stellar center rather than near the limb. Second, at small b_P the moon's orbit across the star is nearly symmetric vertically, and hence is nearly equally likely to miss transit above or below the star (unlike in Figure 2).

The TDVs for small b_P are largely caused by the velocity change effect, which is dependent on the horizontal position of the moon and hence is not strongly correlated with the presence of moon transits.

In Figure 4 we show TTVs and TDVs for three example simulations. The sole change is $b_P = 0.1, 0.4,$ and 0.7 . The

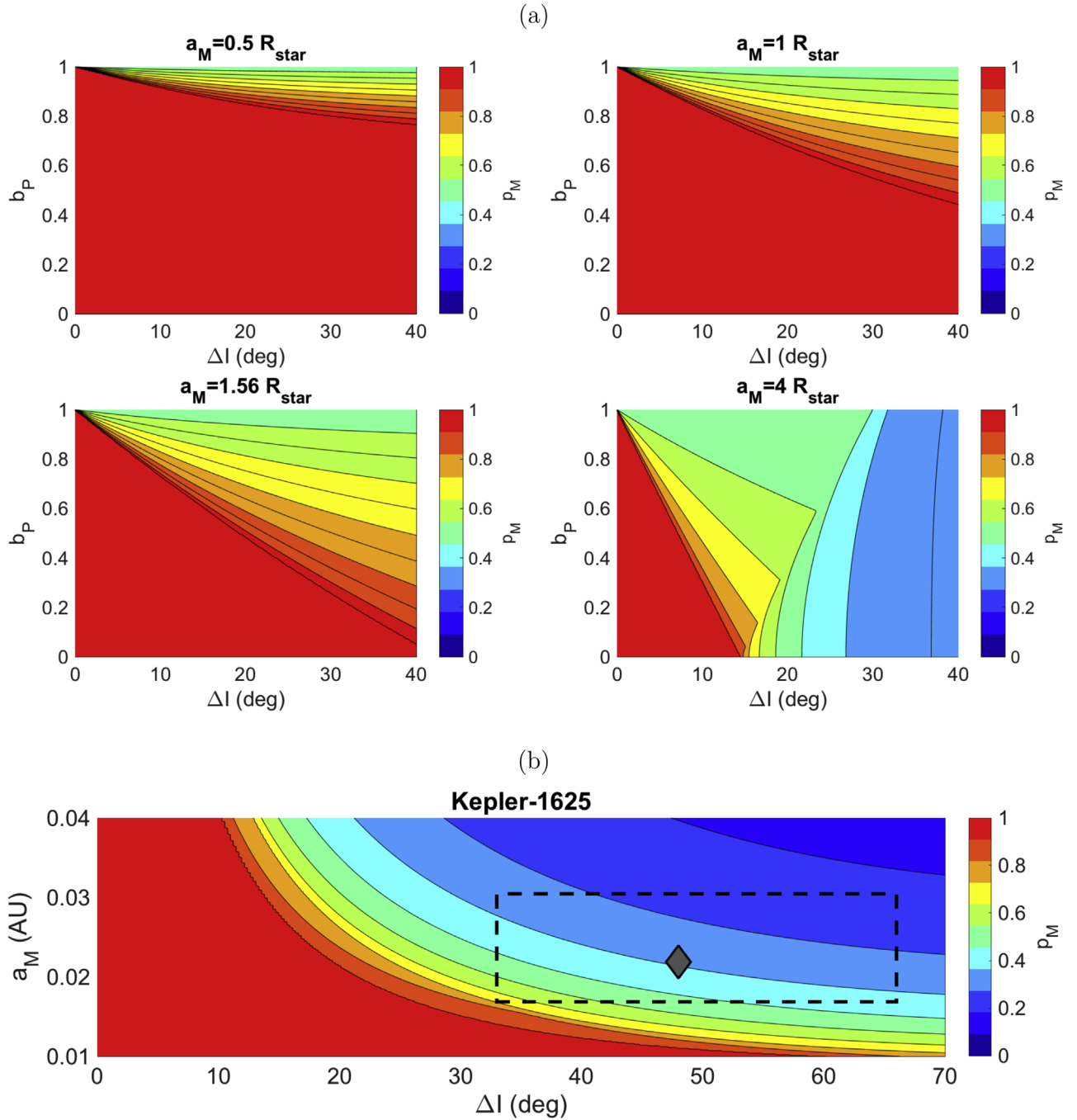


Figure 5. (a) p_M as a function of the planet’s impact parameter b_P , and the mutual inclination, ΔI , for $R_* = 1R_\odot$ and four different values of a_M . (b) p_M of Kepler-1625b-i using the nominal parameters from Teachey & Kipping (2018), where we scan across ΔI and a_M . The gray diamond is the best-fitting value and the dashed boxes are 1σ error bounds. Note that the transit probability is symmetric between prograde and retrograde orbits, and indeed ΔI could be just as likely 132° as its noted value here of 48° . Note that in (b) for ΔI between 40 and 70° there will be Kozai–Lidov cycles, which would affect the true p_M in the long term but are not accounted for in our equations.

planet TTV signal remains constant, although the sequence of moon transits changes. The TDV signal at small b_P is small in amplitude with no correlation with the moon transits. As b_P increases, so does the TDV amplitude and the moon transit correlation.

The impact parameter of the planet Kepler-1625b is well constrained to be small: $b_P = 0.104^{+0.084}_{-0.066}$. We therefore expect TDVs to be small and uncorrelated with missed moon transits, and indeed no TDVs have been observed so far.

4. Applications

4.1. Transit Probability of Hypothetical Exomoon Systems

The transit probability for the moon is a function of ΔI , b_P , and a_M/R_* . Figure 5(a) shows p_M (Equation (7)) over a wide range of parameters: $\Delta I \in [0, 40^\circ]$, $b_P \in [0, 1]$, and $a_M/R_* = 0.5, 1, 1.56, 4$.

For $a_M/R_* < 1.56$ the transit probability is 1 except for high values of ΔI and/or b_P , where the probability goes to a

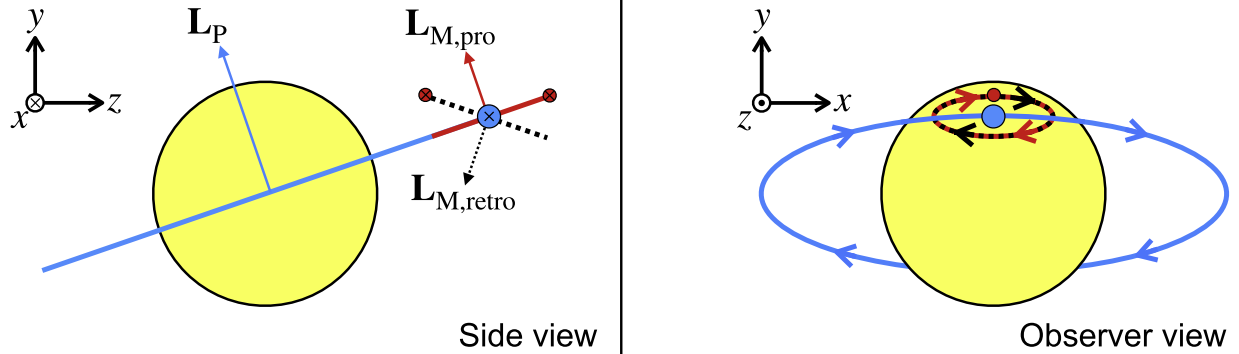


Figure 6. Exoplanet orbit (blue) with two different exomoon orbits: the red solid line is prograde and coplanar to the planet, and the black dashed line is retrograde and misaligned to the planet. As seen by the observer (right) there is a degeneracy, as both moons has the same (x, y) position and (v_x, v_y) velocity, despite the side view (left) betraying a clear difference between the two orbits. L denotes the angular momentum vectors.

minimum of 0.5. The parameter space where $p_M < 1$ increases as a_M/R_* increases. When $a_M/R_* > 1.56$ the moon’s orbit is so wide that its vertical extent exceeds the stellar diameter and $p_M < 0.5$ for some ΔI and b_p .

4.2. Transit Probability of Kepler-1625b-i

In Figure 5(b) we calculate p_M for Kepler-1625b-i over a plausible range of a_M and ΔI , while fixing $b_p = 0.1$ and $R_* = 1R_\odot$. Note that when calculating the nominal value of ΔI we take $\Omega_M = 0^\circ$ and then $\Delta I \approx 90^\circ - I_M$ from Equation (2). This means $\Delta I = 48^\circ$, which places the system just within the nominal Kozai–Lidov regime, but the ΔI and e_M variations should be small enough for our equations to remain applicable.

The Teachey & Kipping (2018) nominal values correspond to $p_M = 0.4$, although this probability varies significantly within the 1σ error bounds, and they note that the moon could still have a coplanar orbit, which would mean $p_M = 1$.

5. Discussion

5.1. Breaking the Prograde/Retrograde Degeneracy

Observations of a moon that orbits a planet on a non-evolving orbit are subject to a degeneracy between prograde ($\Delta I < 90^\circ$) and retrograde ($\Delta I > 90^\circ$) orbits. This degeneracy is shown in Figure 6. Two orbits are shown: one in solid red that is prograde and coplanar ($\Delta I = 0^\circ$, red solid line), and one in dashed black that is retrograde but misaligned ($90^\circ < \Delta I < 180^\circ$). Both orbits yield the same projected x and y positions and v_x and v_y velocities of the moon; hence, the Keplerian TTV and TDV phenomenology would be the same. However, the side view (left) reveals a clear difference in the two moon orientations.

This degeneracy may be broken by nodal precession, which would not occur for the coplanar orbit but would for the misaligned orbit. Fortunately, for a moon that orbits at a fair fraction of its planet’s Hill sphere, precession will be rapid, revealing the magnitude of the misalignment in just tens of orbits of the planet. Therefore, the dynamically evolving character of TDV will betray the prograde or retrograde character of the moon.

If the planetary impact parameter is low then the “TIP–TDV” may be negligible and the magnitude of non-coplanarity may not be enough to break the degeneracy. In this case, higher-order dynamical effects that differ in sign between prograde and retrograde moons may need to be taken into

account, as envisioned by Lewis & Fujii (2014). Two alternative methods for breaking the degeneracy, practical only with Extremely Large Telescopes, were discussed by Heller & Albrecht (2014).

5.2. The Prevalence of Large TTVs for Long-period Gas Giants

According to the transit times of Table S3 of Teachey & Kipping (2018), the planet Kepler-1625b has a mean absolute deviation from a constant-period model, normalized by the orbital period—a “scatter”—of $s_{O-C}/T_P = 2.40 \times 10^{-5}$. The timings have a median error bar normalized by the orbital period of $\sigma/T_P = 1.55 \times 10^{-5}$. For the TTV measurements of Holczer et al. (2016), the data are more precise than that for 40 planets with $T_P > 100$ days. Of those 40, 15 planets have larger TTV scatter, i.e., $s_{O-C}/T_P > 2.40 \times 10^{-5}$, and all of these are deemed significant at $\log p < -8.8$. The large amplitude and period of these signals makes them likely due to planet–planet perturbations. We conclude that Kepler-1625b may very likely have a TTV signal due to additional planets, which may be confused for exomoons, or at least contaminate the exomoon TTV signal. A repeated photometric transit signal of the exomoon, rather than the TTV induced on the planet, is likely a more reliable signature.

5.3. Overlapping Moon and Planet Transits

There are two possible scenarios for overlapping moon and planet transits. First, the moon may be entirely in front of or behind the planet, in which case the photometric signal would be identical to that of an isolated planet transit and the moon would be hidden. Such an event is not explicitly considered in our equations. We estimate it to be rare though, with a likelihood on the order of $\approx R_P/a_M$ if $I_M = I_P = 90^\circ$, and significantly less for inclinations that allow the moon to be offset vertically from the planet at transit. Second, the moon and planet may pass the star at the same time, but with different impact parameters. In this case their photometric dips would be additive and, if telescope precision allowed, a distortion in the transit shape may be detected. Such an event would be covered in our equations for p_M . Exotic syzygies such as this are treated in more detail in Kipping (2011), Veras & Breedt (2017), and Veras (2019).

5.4. Future Observing Prospects

The most effective way to confirm and characterize the Kepler-1625 system is through continued transit photometry. Even if the moon only transits $\approx 40\%$ of the time as we predict, additional planet transits will provide new TTV measurements, although probably not new TDV measurements due to the planet's small impact parameter. The next planet transit is scheduled for 2019 May 26. Figure S18 of Teachey & Kipping (2018) predicts when the moon will transit. Most of their models show a moon transit before the planet's ingress, but they do not quantify the chance of the moon missing transit.⁶


The Transiting Exoplanet Survey Satellite (TESS; Ricker et al. 2014) can feasibly observe the planet transit on 2022 July 19 and 2026 June 25, but at $J_{\text{mag}}=14.4$ the transit will only be observed at a signal-to-noise ratio of 2.5, which is insufficient for transit timing or moon spotting.

The *James Webb Space Telescope (JWST)* will provide superior photometric precision to *HST* (Beichman et al. 2014). From its observing constraints, *JWST* can observe Kepler-1625 annually from April 22 to November 14, meaning the first planet transits observable with this facility will occur on 2021 October 5, 2022 July 19, and 2023 May 3. With *JWST*, the transit timing will likely be limited by our abilities to model the granulation features on the stellar surface, which induce significant correlated noise on ≈ 20 minute timescales given the subgiant nature of this star. Transits of a moon signal of the amplitude and duration claimed by Teachey & Kipping (2018) will be detectable at the 3σ level.

If the moon does not exist, then a binomial test reveals how many non-transits are required to prove this to a certain significance. This assumes that each moon transit would have been detectable and that the transit probability of individual moon transits is independent for each planet transit, which neglects mean motion resonances. The probability of n undetected transits is $p_n = (1 - p_M)^n$. With our estimated $p_M = 0.4$, for a 95%-confident non-detection we solve $(1 - 0.95) = (1 - 0.4)^n$ to obtain $n \sim 6$ well-surveyed yet undetected exomoon transits. If the moon does exist, then a similar number of transits would be also be needed to well characterize its orbit.

The authors are very grateful for the comments of an anonymous referee, which were used to improve this letter.

ORCID iDs

David V. Martin  <https://orcid.org/0000-0002-7595-6360>
 Daniel C. Fabrycky  <https://orcid.org/0000-0003-3750-0183>
 Benjamin T. Montet  <https://orcid.org/0000-0001-7516-8308>

References

- Bashi, D., Helled, R., Zucker, S., & Mordasini, C. 2017, *A&A*, **604**, A83
 Beichman, C., Benneke, B., Knutson, H., et al. 2014, *PASP*, **126**, 1134
 Bennett, D. P., Batista, V., Bond, I. A., et al. 2014, *ApJ*, **785**, 155
 Boué, G., & Laskar, J. 2006, *Icar*, **185**, 312
 Burns, J. A. 1986, in *Satellites*, ed. J. A. Burns & M. S. Matthews (Tucson, AZ: Univ. Arizona Press), 117
 Forgan, D. 2018, *RNAAS*, **2**, 191
 Heller, R. 2014, *ApJ*, **787**, 14
 Heller, R. 2018, *A&A*, **610**, A39
 Heller, R., & Albrecht, S. 2014, *ApJL*, **796**, L1
 Heller, R., Hippke, M., Plavec, B., Angerhausen, D., & Agol, E. 2016, *A&A*, **591**, A67
 Heller, R., Marleau, G.-D., & Pudritz, R. E. 2015, *A&A*, **579**, L4
 Heller, R., Rodenbeck, K., & Bruno, G. 2019, arXiv:1902.06018
 Holczer, T., Mazeh, T., Nachmani, G., et al. 2016, *ApJS*, **225**, 9
 Hwang, K.-H., Udalski, A., Bond, I. A., et al. 2018, *AJ*, **155**, 259
 Kegerreis, J. A., Teodoro, L. F. A., Eke, V. R., et al. 2018, *ApJ*, **861**, 52
 Kipping, D. M. 2009a, *MNRAS*, **392**, 181
 Kipping, D. M. 2009b, *MNRAS*, **396**, 1797
 Kipping, D. M. 2011, *MNRAS*, **416**, 689
 Kipping, D. M., Fossey, S. J., & Campanella, G. 2009, *MNRAS*, **400**, 398
 Kozai, Y. 1962, *AJ*, **67**, 579
 Laskar, J., Joutel, F., & Robutel, P. 1993, *Natur*, **361**, 615
 Lewis, K., & Fujii, Y. 2014, *ApJL*, **791**, L26
 Lewis, K. M., Ochiai, H., Nagasawa, M., & Ida, S. 2015, *ApJ*, **805**, 27
 Lidov, M. 1962, *P&SS*, **9**, 719
 Lidov, M. L. 1961, *Iskusst. Sputniki Zemli*, **8**, 5
 Mardling, R. A. 2010, *MNRAS*, **407**, 1048
 Martin, D. V. 2017, *MNRAS*, **467**, 1694
 Namouni, F. 2010, *ApJL*, **719**, L145
 Ricker, G., Winn, J., Vanderspek, R., et al. 2014, *Proc. SPIE*, **9143**, 20
 Ronnet, T., Mousis, O., Vernazza, P., Lunine, J. I., & Crida, A. 2018, *AJ*, **155**, 224
 Sartoretti, P., & Schneider, J. 1999, *A&AS*, **134**, 553
 Sengupta, S., & Marley, M. S. 2016, *ApJ*, **824**, 76
 Simon, A., Szabó, G., Kiss, L., & Szatmáry, K. 2012, *MNRAS*, **419**, 164
 Teachey, A., & Kipping, D. M. 2018, *SciA*, **4**
 Teachey, A., Kipping, D. M., & Schmitt, A. R. 2017, *AJ*, **155**, 36
 Tremaine, S., Touma, J., & Namouni, F. 2009, *AJ*, **137**, 3706
 Vanderburg, A., Rappaport, S. A., & Mayo, A. W. 2018, *AJ*, **156**, 184
 Veras, D. 2019, *MNRAS*, **483**, 3919
 Veras, D., & Breedt, E. 2017, *MNRAS*, **468**, 2672

⁶ At the American Astronomical Society Meeting 233, Seattle, 2019 January, Alex Teachey's presentation noted a simulated moon transit chance of 53% for 2019 May. This is slightly above our 40% analytic calculation, but our calculations are an average over all transit epochs, not any specific one.